This article was downloaded by:
On: *25 January 2011*
Access details: *Access Details: Free Access*
Publisher *Taylor & Francis*
Informa Ltd Registered in England and Wales Registered Number: 1072954 Registered office: Mortimer House, 37-41 Mortimer Street, London W1T 3JH, UK

Liquid Crystals
Publication details, including instructions for authors and subscription information:
http://www.informaworld.com/smpp/title~content=t713926090

Novel chiral calamitic liquid crystalline oxadiazoles as ferroelectric materials

M. L. Parra[a]; P. I. Hidalgo[a]; E. A. Soto-Bustamante[b]; J. Barberá[c]; E. Y. Elgueta[a]; V. H. Trujillo-Rojo[b]
[a] Facultad de Ciencias Químicas, Departamento de Química Orgánica, Universidad de Concepción, Concepción, Chile [b] Facultad de Ciencias Químicas y Farmacéuticas, Universidad de Chile, Santiago, Chile [c] Facultad de Ciencias-Instituto de Ciencia de Materiales de Aragón, Química Orgánica, Universidad de Zaragoza-C.S.I.C., 50009, Zaragoza, Spain

To cite this Article Parra, M. L. , Hidalgo, P. I. , Soto-Bustamante, E. A. , Barberá, J. , Elgueta, E. Y. and Trujillo-Rojo, V. H.(2008) 'Novel chiral calamitic liquid crystalline oxadiazoles as ferroelectric materials', Liquid Crystals, 35: 10, 1251 — 1262
To link to this Article: DOI: 10.1080/02678290802513790
URL: http://dx.doi.org/10.1080/02678290802513790

PLEASE SCROLL DOWN FOR ARTICLE

Full terms and conditions of use: http://www.informaworld.com/terms-and-conditions-of-access.pdf

This article may be used for research, teaching and private study purposes. Any substantial or systematic reproduction, re-distribution, re-selling, loan or sub-licensing, systematic supply or distribution in any form to anyone is expressly forbidden.

The publisher does not give any warranty express or implied or make any representation that the contents will be complete or accurate or up to date. The accuracy of any instructions, formulae and drug doses should be independently verified with primary sources. The publisher shall not be liable for any loss, actions, claims, proceedings, demand or costs or damages whatsoever or howsoever caused arising directly or indirectly in connection with or arising out of the use of this material.

Liquid Crystals,
Vol. 35, No. 10, October 2008, 1251–1262

Taylor & Francis
Taylor & Francis Group

Novel chiral calamitic liquid crystalline oxadiazoles as ferroelectric materials

M. L. Parra[a]*, P. I. Hidalgo[a], E. A. Soto-Bustamante[b], J. Barberá[c], E. Y. Elgueta[a] and V. H. Trujillo-Rojo[b]

[a]*Facultad de Ciencias Químicas, Departamento de Química Orgánica, Universidad de Concepción, PO Box 160-C, Concepción, Chile;* [b]*Facultad de Ciencias Químicas y Farmacéuticas, Universidad de Chile, PO Box 233, Santiago, Chile;* [c]*Facultad de Ciencias-Instituto de Ciencia de Materiales de Aragón, Química Orgánica, Universidad de Zaragoza-C.S.I.C., 50009, Zaragoza, Spain*

(Received 2 June 2008; final form 26 September 2008)

Novel liquid crystalline materials based on chiral calamitic 1,2,4- and 1,3,4-oxadiazole derivatives were synthesized and their thermotropic mesomorphism investigated by polarizing optical microscopy and differential scanning calorimetry. The structures of their smectic phases were investigated by X-ray diffraction. The existence of ferroelectric properties in the smectic C phase was also studied.

Keywords: ferroelectric liquid crystals; oxadiazole derivatives; mesomorphism

Downloaded At: 15:02 25 January 2011

1. Introduction

It is well known that mesogens made from optically active molecules can form chiral mesophases exhibiting ferroelectricity (*1*). Ferroelectric liquid crystals (FLCs) have attracted considerable interest due to their unique properties and their potential technical applications (*2–4*). Meyer *et al.* (*5*) first reported the phenomenon of ferroelectricity in a chiral smectic C (SmC*) mesophase in 1975. Clark and Lagerwall (*1*) found a new electro-optical effect in surface-stabilized ferroelectric liquid crystals (SSFLCs) and academic and technological research in FLCs began to receive much more attention, owing to their potential application in fast switching devices; they are also potential candidates for nonlinear optics and photonic applications (*6–9*).

Our interest in the relationship between molecular structure and mesomorphic and ferroelectric behaviour has led us to design new chiral molecules that incorporate a five-membered heterocycle in the mesogenic core (*10, 11*). Only a few examples of this type of structure in FLCs have been reported in the literature and these include chiral 1,3,4-thiadiazole (*10–13*), chiral pyrazole and isoxazole (*14*) and chiral 1,2,3-triazole (*15, 16*) derivatives. Other five-membered heterocyclic compounds, such as 1,3,4- and 1,2,4-oxadiazoles have also proven to be highly efficient in promoting mesomorphic properties, especially the 1,3,4-oxadiazoles (*17–31*). The latter have been shown to exhibit novel properties (*32–36*), focused on electron-transporting or photoconducting capability for advance electronic devices. For example, non-mesomorphic 2,5-bis-(4-naphtyl)-1,3,4-oxadiazole has been reported to be one of the best organic electron conductors (*32*). Mesomorphic oxadiazole derivatives are generally achiral calamitic molecules (*15–28*), exhibiting nematic/smectic phases and electron-transporting capability (*27–30*).

Non-chiral mesomorphic compounds containing the 1,3,4-oxadiazole ring, which have been reported in our previous communications (*17, 37–39*), display a broad temperature range of tilted smectic phase. In addition, we have reported a new series of 1,2,4-oxadiazole-based compounds exhibiting smectic A (SmA) and/or nematic (N) phases (*40*). A variety of mesogenic 1,2,4-oxadiazoles have been synthesized by Torgova *et al.* (*41*). More recently, we have reported the first chiral calamitic liquid crystals based on 1,2,4- and 1,3,4-oxadiazole heterocycles (*42*) (see Figure 1). Both 1,3,4- and 1,2,4-oxadiazole rings can contribute significantly to the molecular dipole in a molecule, owing to the high dipole moment contained in the plane of the heterocycle. All these aspects are relevant in the design of new chiral compounds as FLCs.

In this paper, as part of our continuing research on heterocyclic mesogens design, we describe the synthesis, mesomorphism and ferroelectric properties of chiral calamitic 1,3,4- and 1,2,4-oxadiazole derivatives. In order to achieve the non-centrosymmetry in the SmC phase necessary for ferroelectric behaviour, one of the terminal groups, attached to the biphenyl moiety, is always a chiral alkoxy chain derived from (*R*)-2-octanol. The other terminal substituent is an achiral thioether chain (compound **I**) and an achiral alkoxy chain (compounds **II** and **III**) with the proviso that the total number of carbon atoms for these achiral terminal substituents must remain as 12. To our knowledge, the prepared

*Corresponding author. Email: mparra@udec.cl

ISSN 0267-8292 print/ISSN 1366-5855 online
© 2008 Taylor & Francis
DOI: 10.1080/02678290802513790
http://www.informaworld.com

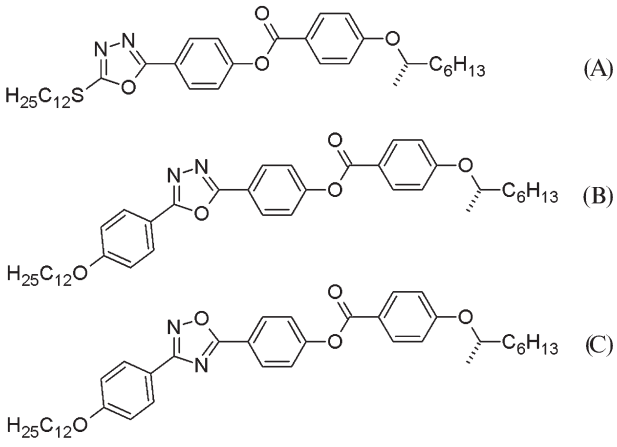

Figure 1. Structure of reported chiral oxadiazoles **A**, **B** and **C**.

compounds are the first chiral calamitic liquid crystals derived from 1,3,4- and 1,2,4-oxadiazole exhibiting ferroelectric properties.

Downloaded At: 15:02 25 January 2011

2. Experimental

Characterization

Infrared spectra were recorder with a Nicolet model 550 spectrometer. ^{1}H and ^{13}C NMR spectra were obtained with a Bruker AC-250P spectrometer at 250 MHz and 62.9 MHz, respectively, using TMS as the internal standard. The melting points, thermal transitions and liquid crystal textures were observed using an Ortholux Pol BK-11 polarizing optical microscope equipped with a Mettler FP 800 hot stage. Thermotropic mesomorphism was investigated by differential scanning calorimetry (DSC) employing a Rheometric DSC-V calorimeter. Samples were encapsulated in aluminium pans and studied at heating/cooling rates of $10^{\circ}C\,min^{-1}$. The instrument was calibrated using an indium standard ($156.6^{\circ}C$, $28.44\,J\,g^{-1}$). The mesophases were investigated by X-ray diffraction. XRD patterns were obtained with a pinhole camera (Anton-Para) operating with a point-focused Ni-filtered Cu K_{α} beam. Powder samples were held in Lindemann glass capillaries (1 mm diam.) and heated with a variable temperature oven. The patterns were collected on flat photographic films, with the capillary axis and film perpendicular to the X-ray beam; spacings were obtained via Bragg's law. Elemental analyses were obtained using a Perkin-Elmer 240 B instrument.

Ferroelectric measurements

Ferroelectric properties were assessed by introducing the liquid crystals into a commercial LC4-6.8 INSTEC sandwich cells with a thickness of 6.8 μm and anti-parallel alignment. They were filled by capillarity in the isotropic state. The cells were placed inside a temperature-controlled thermal oven (Instec MK2) that allows a temperature control ranging from $0.1^{\circ}C\,min^{-1}$ up to $20^{\circ}C\,min^{-1}$. The temperature range was from $-170^{\circ}C$ to $200^{\circ}C$. The heating or cooling process was monitored with an IBM PC-compatible computer.

The electric displacement, D, was determined by the field reversal method (*43*). A square wave voltage of 70 Hz was applied to the sample cell and the electric displacement current was monitored on an oscilloscope HP 56000 linked to a PC through a GPIB card. The curves were stored in the PC for further data processing. The time switching was obtained directly from the time scale, at the polarization peak. The corresponding spontaneous polarization was determined using the triangular wave method (*44*) applying a voltage of $200\,V_{pp}$ and 70 Hz to the sample cell. The polarization current, also followed with the oscilloscope and stored in the PC, can be easily obtained by subtracting the capacitive and ohmic components and taking into account the electrode areas.

Materials and synthesis

All reagents were obtained from commercial sources and used without further purification. The organic solvents were commercial-grade quality and all were dried by traditional methods. In general, all compounds were purified by column chromatography on silica gel (60–120 mesh), centrifugal thin-layer chromatography (Chromatotron 8924) and crystallization from analytical grade solvents. The purity of the compounds was checked by thin-layer chromatography (Merck Kieselgel 60F254). Precursors **1**, **2** and **4** (see Scheme 1) were synthesized according to the procedure described in previously (*38, 40*).

*5-(4-hydroxyphenyl)-2-(4-n-dodecyloxyphenyl)-1,3,4-oxadiazole (**3**).*

To a mixture of 1.95 mmol of compound **2**, cyclohexene (8 ml) and ethanol (16 ml), $Pd(OH)_2/C$ (20%) (0.1 g) was added in small portions under a nitrogen atmosphere. The mixture was heated at reflux for 24 h, filtered through a pad of Celite and the solvent evaporated. The crude product was purified by recrystallization in ethanol. Yield 85% of a white solid, m.p. $134^{\circ}C$. ^{1}H NMR (250 MHz, TMS, $CDCl_3$): δ 0.80 (t, 3H, CH_3), 1.21–1.70 (m, 20H, aliph. chain), 4.03 (t, 2H, OCH_2), 6.05 (s, 1H, OH), 6.96 (d, J=7.84 Hz, 2H, arom. H), 7.11 (d, J=7.95 Hz, 2H, arom. H), 7.92 (d, J=7.79 Hz, 2H,

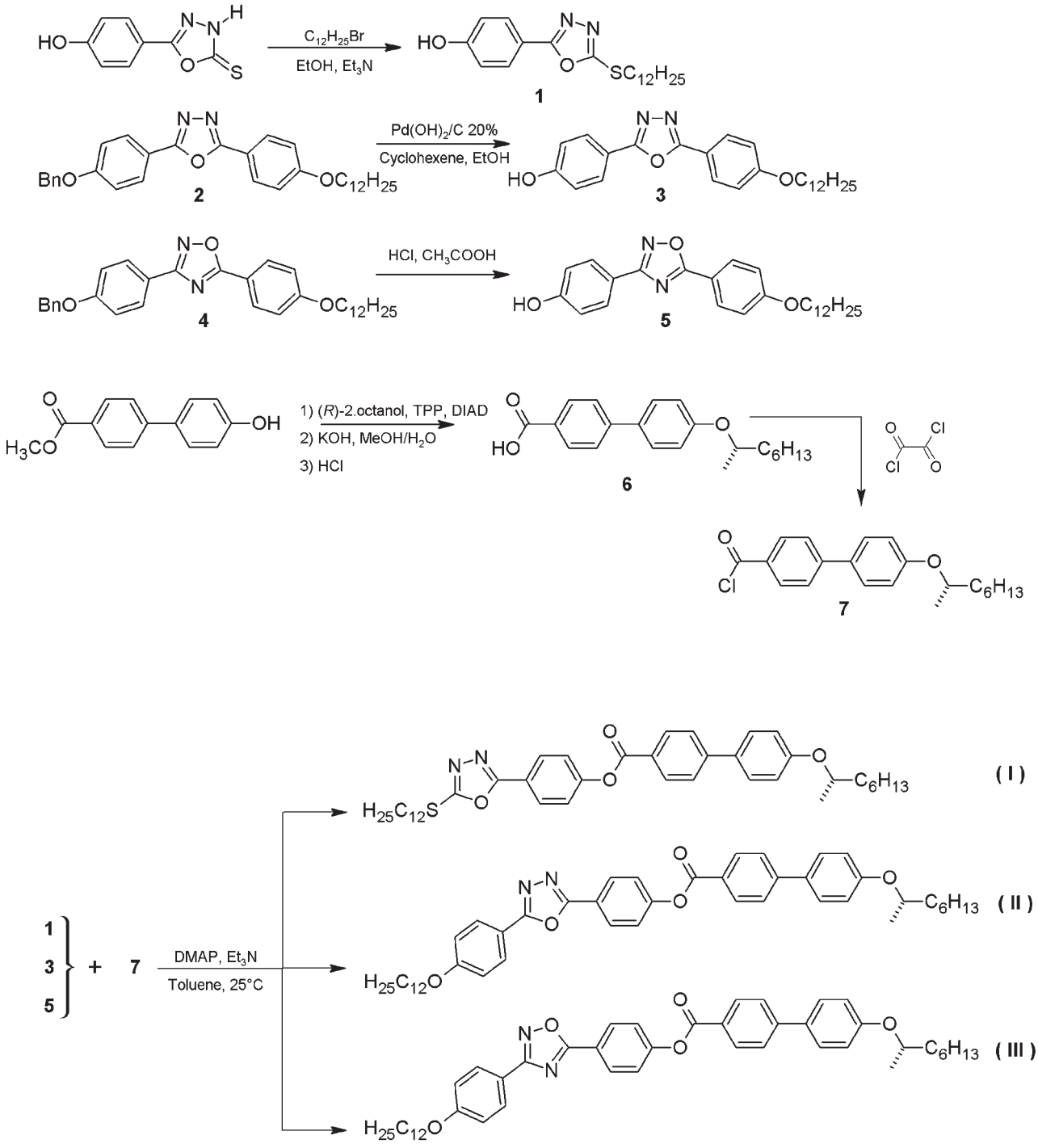

Scheme 1. Synthesis of chiral calamitic 1,2,4- and 1,3,4-oxadiazole derivatives (TPP is triphenylphosphine, DIAD is diisopropylazodicarboxylate and DMAP is dimethylaminopyridine).

arom. H), 7.98 (d, J=7.94 Hz, 2H, arom. H). ^{13}C NMR (62.9 MHz, TMS, $CDCl_3$): δ 13.8, 22.0, 25.3, 28.4, 28.6, 28.9, 31.2 (aliph. C), 67.8 ($O\underline{C}H_2$), 115.2, 116.1, 128.2, 128.4 (arom. CH), 114.2, 115.7, 160.7, 161.3, 163.2, 163.6. (quaternary arom. C). IR (KBr disk, cm^{-1}): 3109 (O–H), 2924 (Csp^3–H), 1606 (C=C), 1255 (C–O).

*5-(4-hydroxyphenyl)-3-(4-n-dodecyloxyphenyl)-1,2,4-oxadiazole (**5**).*

A mixture of 0.78 mmol of compound **4**, 12 ml of glacial acetic acid and 6 ml of hydrochloride acid was heated under reflux for 6 h. The mixture was poured into water/ice and was neutralized with aqueous NaOH. The crude product was filtered and washed

Downloaded At: 15:02 25 January 2011

with water. The product was recrystallized from *n*-hexane. Yield 83% of a white solid, m.p. 110–113°C. ^{1}H NMR (250 MHz, TMS, $CDCl_3$): δ 0.80 (t, 3H, CH_3), 1.25–1.73 (m, 20H, aliph. chain), 3.95 (t, 2H, OCH_2), 6.13 (s, 1H, OH), 6.88 (d, J=8.75 Hz, 2H, arom. H), 6.94 (d, J=7.04 Hz, 2H, arom. H), 7.96 (d, J=8.76 Hz, 2H, arom. H), 8.05 (d, J=6.97 Hz, 2H, arom. H). ^{13}C NMR (62.9 MHz, TMS, $CDCl_3$): δ 14.1, 22.7, 26.0, 29.3, 29.6, 31.9 (aliph. C), 70.1 ($O\underline{C}H_2$), 114.9, 115.8, 129.4, 130.0 (arom. CH), 116.2, 119.5, 157.8, 163.5, 168.1, 175.8 (quaternary arom. C). IR (KBr disk, cm^{-1}): 3412 (O–H), 2922 (Csp^3–H), 1610 (C=C), 1251 (C–O).

*(S)-4′-(1″-methylheptyloxy)-4-biphenylcarboxylic acid (**6**).*

To a solution of methyl 4′-hydroxy-4-biphenylcarboxylate (6.30 mmol) and triphenylphosphine (TPP) (9.45 mmol) in dry THF (25 ml) was added 9.45 mmol of (*R*)-2-octanol dissolved in 20 ml of dry THF. Diisopropylazodicarboxylate (DIAD) (9.45 mmol) in 70 ml of dry THF was then added dropwise. The mixture was stirred for 24 h at room temperature under nitrogen atmosphere. Then the solvent was evaporated and the residue was dissolved in 80 ml of *n*-hexane/ethyl acetate (7:3) and stirred for 1 h at room temperature, and the triphenylphosphine oxide formed was removed by filtration. The methyl ester was obtained in solid form after evaporation of the filtrate and was used in saponification reaction without further purification. The purity of this compound was evaluated by TLC. This product was saponified using an excess of KOH in a methanol/water (2:1) solution under reflux for 8 h. The solution was cooled, diluted with water and acidified with HCl. The chiral acid **6** was recrystallized from ethanol. Yield 96% of white solid, Cr 162°C SmC* 175°C N* 194°C I. ^{1}H NMR (250 MHz, TMS, $CDCl_3$): δ 0.84 (t, 3H, CH_3), 1.25–2.08 (m, 13H, $5CH_2$ and $C\underline{H}_3CH$), 4.49 (m, 1H, $C\underline{H}CH_3$), 7.01 (d, J=7.01 Hz, 2H, arom. H), 7.65 (d, J=7.65 Hz, 2H, arom. H), 7.73 (d, J=7.73 Hz, 2H, arom. H), 7.98 (d, J=7.97 Hz, 2H, arom. H), 12,90 (s, 1H, COOH). ^{13}C NMR (62.9 MHz, TMS, $CDCl_3$): δ 14.1, 19.7, 22.6, 25.5, 29.2, 31.7, 36.4 (aliph. C), 74.0 (O$\underline{C}$H chiral chain), 116.1, 126.5, 128.4, 130.7 (arom. CH), 127.1, 131.4, 146.1, 158.6, 171.9 (quaternary arom. C). IR (KBr disk, cm^{-1}): 3100–3000 (O–H), 1668 (C=O), 1248 (C–O).

*(S)-4′-(1″-methylheptyloxy)-4-biphenylcarboxylic acid chloride (**7**).*

1 mmol of the chiral acid **6** in 20 ml of dry CH_2Cl_2 was cooled at 0°C in an ice bath and an excess of oxalyl chloride was then added. The mixture was stirred at room temperature for 4 h. The resulting chiral acid chloride (**7**) was obtained in liquid form after evaporation of the solvent and of the excess of oxalyl chloride and was used in subsequent reaction without further purification.

General procedure for synthesis of the esters (I–III)

To a mixture of 1 mmol of the corresponding phenol (**1**, **3**, **5**), 0.032 g of DMAP, 1 ml of dry triethylamine and 35 ml of dry toluene, 1 mmol of the chiral acid chloride **7** was added. The mixture was stirred at room temperature for 24 h. The resulting mixture was diluted with ether (30 ml). The organic solution was washed twice with water (30 ml) and once with 20 ml of brine. The organic phase was dried over Na_2SO_4, filtered off and the solvent was evaporated and the residue was purified by column chromatography, circular chromatography and recrystallization from ethanol.

*(S)-4-[5-(n-dodecylthio)-1,3,4-oxadiazole-2-yl]phenyl 4′-(1″-methylheptyloxy)biphenyl-4-carboxylate (**I**).*

The crude product was chromatographed (silica gel: *n*-hexane–ethyl acetate 4:1 and circular chromatography, Chromatotron: dichlorometane) and recrystallized from ethanol. Yield 44% of a white solid. ^{1}H NMR (250 MHz, TMS, $CDCl_3$): δ 0.88 (2t, 6H, $2CH_3$), 1.26–1.33 (m, 22H, aliph. chain), 1.36 (d, 3H, CH_3 of the chiral chain), 1.41–1.88 (m, 8H, aliph. chain), 3.31 (t, 2H, SCH_2), 4.44 (m, 1H, $OC\underline{H}CH_3$), 7.01 (d, J=6.82 Hz, 2H, arom. H), 7.38 (d, J=6.76 Hz, 2H, arom. H), 7.57 (d, J=6.79 Hz, 2H, arom. H), 7.69 (d, J=6.81 Hz, 2H, arom. H), 8.08 (d, J=6.78 Hz, 2H, arom. H), 8.24 (d, J=6.74 Hz, 2H, arom H). ^{13}C NMR (62.9 MHz, TMS, $CDCl_3$): δ 14.1, 19.7, 22.6, 22.7, 25.5, 28.5, 29.0, 29.2, 29.4, 29.6, 31.7, 31.9, 32.6, 36.4 (aliph. C), 74.0 (O$\underline{C}$H–), 116.1, 122.6, 126.6, 128.0, 128.4, 130.7 (arom. CH), 121.3, 126.8, 131.6, 146.3, 153.5, 158.7, 164.4 (quaternary arom. C), 164.6 (C=O). IR (KBr disk, cm^{-1}): 2924 (Csp^3–H), 1735 (C=O), 1601 (C=C), 1253 (C–O). Elemental analysis: calculated for $C_{41}H_{54}N_2O_4S$, C 73.39, H 8.11, N 4.18, S 4.78; found, C 72.62, H 8.27, N 4.33, S 4.02%.

*(S)-4-[5-(4-n-dodecyloxyphenyl)-1,3,4-oxadiazole-2-yl]phenyl 4′-(1″-methylheptyloxy)-biphenyl-4-carboxylate (**II**).*

The crude product was chromatographed (silica gel: *n*-hexane–ethyl acetate 9:1 and circular chromatography, Chromatotron: *n*-hexane–dichlorometane

Downloaded At: 15:02 25 January 2011

2:1) and recrystallized from ethanol. Yield 70%, of a white solid. ^{1}H NMR (250 MHz, TMS, $CDCl_3$): δ 0.88 (2t, 6H, $2CH_3$), 1.26–1.33 (m, 22H, aliph. chain), 1.37 (d, 3H, CH_3 of the chiral chain), 1.39–1.85 (m, 8H, aliph. chain), 4.08 (t, 2H, OCH_2), 4.45 (m, 1H, $OCHCH_3$), 6.97 (d, J=8.77 Hz, 2H, arom. H), 7.04 (d, J=8.62 Hz, 2H, arom. H), 7.43 (d, J=8.76 Hz, 2H, arom. H), 7.61 (d, J=8.76 Hz, 2H, arom. H), 7.72 (d, J=8.54 Hz, 2H, arom. H), 8.17 (d, J=8.78 Hz, 2H, arom. H), 8.29 (d, J=8.55 Hz, 4H, arom. H). ^{13}C NMR (62.9 MHz, $CDCl_3$): δ 14.1, 19.8, 22.6, 22.7, 25.5, 25.9, 29.1, 29.3, 29.6, 31.8, 31.9, 36.5 (aliph. C), 68.6 (OCH_2), 74.1 (OCH–), 115.1, 116.4, 122.2, 126.6, 128.4, 128.8, 130.1, 130.8 (arom. CH), 116.5, 124.5, 127.2, 131.4, 146.4, 152.9, 158.7, 162.6, 164.5, 168.1 (quaternary arom. C), 172.6 (C=O). IR (KBr disk, cm^{-1}): 2923 (Csp^3–H), 1726 (C=O), 1611 (C=C), 1256 (C–O). Elemental analysis: calculated for $C_{47}H_{58}N_2O_5$, C 77.23, H 8.00, N 3.83; found, C 76.45, H 8.15, N 3.98%.

*(S)-4-[5-(4-n-dodecyloxyphenyl)-1,2,4-oxadiazole-3-yl)phenyl 4′-(1″-methylheptyloxy)-biphenyl-4-carboxylate (**III**).*

The crude product was chromatographed (silica gel: *n*-hexane–ethyl acetate 9:1 and circular chromatography, Chromatotron: *n*-hexane–dichloromethane 1:1) and recrystallized from ethanol. Yield 85%, of a white solid. ^{1}H NMR (250 MHz, TMS, $CDCl_3$): δ 0.89 (2t, 6H, $2CH_3$), 1.29–1.34 (m, 22H, aliph. chain), 1.37 (d, 3H, CH_3 of the chiral chain), 1.40–1.88 (m, 8H, aliph. chain), 4.07 (t, 2H, OCH_2), 4.46 (m, 1H, $OCHCH_3$), 6.99 (d, J=8.72 Hz, 2H, arom. H), 7.06 (d, J=8.64 Hz, 2H, arom. H), 7.42 (d, J=8.74 Hz, 2H, arom. H), 7.61 (d, J=8.76Hz, 2H, arom. H), 7.72 (d, J=8.50 Hz, 2H, arom. H), 8.16 (d, J=8.91 Hz, 2H, arom. H), 8.29 (d, J=8.55 Hz, 4H, arom. H). ^{13}C NMR (62.9 MHz, TMS, $CDCl_3$): δ 14.1, 19.8, 22.6, 22.7, 25.5, 25.9, 29.1, 29.3, 29.6, 31.8, 31.9, 36.5 (aliph. C), 68.4 (OCH_2), 74.1 (OCH–), 114.9, 116.2 122.2, 126.6, 128.4, 128.8, 130.1, 130.8 (arom. CH), 116.5, 124.8, 127.2, 131.4, 146.4, 152.9, 158.7, 162.6, 164.5, 168.1 (quaternary arom. C), 172.6 (C=O). IR (KBr disk, cm^{-1}): 2922 (Csp^3–H), 1730 (C=O), 1606 (C=C), 1256 (C–O). Elemental analysis: calculated for $C_{47}H_{58}N_2O_5$, C 77.23, H 8.00, N 3.83; found, C 77.01, H 8.11, N 3.95%.

3. Results and discussion

Synthesis

The synthetic procedures used to prepare compounds **I**–**III** are shown in Scheme 1. Synthesis and analytical data for oxadiazole derivatives **1**, **2** and **4**, which are precursors of the new materials, were reported previously (*38, 40*). The benzyl group (Bn) in oxadiazoles **2** and **4** was removed using standard synthetic procedures (*14*) leading to the formation of the corresponding phenolic 1,3,4- and 1,2,4-oxadiazole (**3** and **5**, respectively). The synthesis of the chiral compound **6** was achieved by the Mitsunobu (*45*) reaction, accomplished under N_2 atmosphere, starting from methyl 4′-hydroxy-4-biphenylcarboxylate and (*R*)-2-octanol. The chiral mesomorphic oxadiazoles **I**–**III** were obtained by esterification of compound **7** with the corresponding phenolic oxadiazole derivatives (**1**, **3** and **5**) according to the procedure described elsewhere (*38*).

Mesomorphic properties

The thermal transitions of the compounds **I**–**III** were studied by polarizing optical microscopy (POM) and DSC. Phase transition temperatures observed by POM agree well with the corresponding DSC thermograms. The phase transitions and thermodynamic data for compounds **I**–**III** are summarized in Table 1 and a graphical representation of the mesomorphic behaviour is presented in Figure 2, in which transition temperatures obtained both on heating and on cooling are shown.

As can be seen from Table 1 and Figure 2, compounds **I**–**III** exhibit enantiotropic mesomorphic behaviour, where the observed phase sequences are Cr–SmC*–SmA–N*–I for **I**, Cr–SmC*–N*–I for **II** and Cr–SmC*–N*–I for **III**. On cooling, a monotropic blue phase (BP) was also observed for compounds **II** and **III**, which appears in a very narrow temperature range (2.0°C and 4.2°C for compound **II** and **III**, respectively). All melting temperatures were in the range 61.2–122.1°C and increased in the order **I** (61.2°C)–**III** (80.6°C)–**II**

Table 1. Phase behaviour of compounds **I**–**III**. The transition temperatures (°C) and enthalpies (in parentheses, $J\,g^{-1}$) were determined by DSC on heating and cooling at a scan rate of $10°C\,min^{-1}$.

Compound	Phase transitions
I	Cr 61.2 (65.9) SmC* 129.0[a] SmA 149.0[a] N* 154.5 (5.6) I
	I 152.4 (5.3) N* 147.0[a] SmA 126.0[a] SmC* 43.4 (58.2) Cr
II	Cr 122.1 (53.2) SmC* 149.3 (1.5) N* 171.2 (0.4) I
	I 171.0[a] BP 169.1 (0.6) N* 148.1 (1.3) SmC* 112.6 (9.4) Cr
III	Cr 80.6 (41.6) SmC* 113.6 (1.7) N* 202.7 (1.8) I
	I 199.6[a] BP 194.5 (1.0) N* 111.3 (1.3) SmC* 53.9 (33.4) Cr

[a]Represents an optical microscopy data. Cr=crystalline phase; SmC*=chiral smectic C phase; SmA=smectic A phase; N*=chiral nematic phase; BP=blue phase; I=isotropic liquid.

Downloaded At: 15:02 25 January 2011

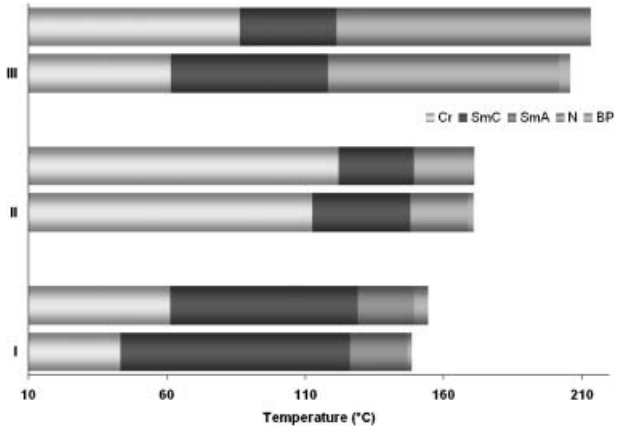

Figure 2. Plots of the mesomorphic behaviour of compounds **I**, **II** and **III**.

(122.1°C). The clearing temperatures were observed at 154.5°C, 202.7°C and 171.2°C, respectively, with compound **III** having the higher mesomorphic temperature range (122.1°C). Compound **I** has a broader SmC* phase range (67.8°C) than compounds **II** and **III** (27.2 and 33°C, respectively), whereas the later compounds have a broader N* phase range (21.9 and 89.1°C, respectively) than compound **I** (5.5°C). As mentioned above, compound **I** also displays a SmA mesophase. Thus, the smectogenic order is much more significant for compound **I**. The differences between 1,3,4-oxadiazole derivatives **I** and **II** can be explained if it is assumed that the bend in the molecular shape is reduced to a certain degree when the oxadiazole ring is shifted to the terminal position of the rigid aromatic core. In this position the flexible thioalkyl chain allows the partial compensation of the molecular bend (*18*).

If we compare compound **II** with compound **III**, the only structural difference is related with the heterocyclic ring, in one case 1,3,4-oxadiazole (**II**) and the other case 1,2,4-oxadiazole (**III**). Thus, the mesomorphic behaviour strongly depends on the nature of the heterocyclic ring in the molecule.

Compound **III** has a lower melting temperature and higher clearing temperature, therefore higher mesomorphic thermal stability, than its structural isomer **II**. This should mainly be due to the deviation of the molecular shape from linearity, which is much more significant for 1,3,4-oxadiazoles and is especially strong if the oxadiazole ring occupies a central position of the rigid aromatic core. From previous studies reported by Torgova *et al.* (*46*), it is known that 2,5-disubstituted 1,3,4-oxadiazole and 3,5-disubstituted 1,2,4-oxadiazole derivatives have an exocyclic bond angle of 134° and 140°, respectively, indicating that the 1,3,4-oxadiazole in the central rigid core produces a greater distortion of the linearity of the molecules when compared with the 1,2,4-oxadiazole derivatives. This deviation from the typical rod-like mesogen shape could explain the differences in the mesomorphic temperature ranges of the compounds reported here.

As mentioned above, recently we have reported chiral liquid crystals with an oxadiazole ring in the mesogenic core (*42*), i.e. compounds **A**, **B** and **C** (see Figure 1). These compounds have the same achiral thioalkyl chain (compound **A**), the same achiral alkoxy chain (compounds **B** and **C**) and the same chiral alkoxy chain derived from chiral *2*-octanol as those of the compounds **I**–**III**. The main difference is in the central rigid core. The replacement of the chiral 1-methylheptyloxyphenyl moiety, present in compounds **A**, **B** and **C**, by a chiral 1-methylheptyloxybiphenyl moiety in compounds **I**, **II** and **III** produces important changes in the mesomorphic behaviour. The compounds reported previously (**A**, **B** and **C**, Figure 1) displayed a monotropic SmC* phase (compounds **A** and **B**) and an enantiotropic N* phase (compound **C**), whereas the compounds reported here (**I**–**III**) display enantiotropic mesomorphism, i.e. SmC*–SmA–N* (compound **I**) and SmC*–N* (compounds **II** and **III**). In addition, a monotropic BP is observed for compounds **II** and **III** (see Table 1 and Figure 2). Clearly, the biphenyl group plays an important role in the stabilization or in the appearance of the mesophases, indicating that the intermolecular interactions are more favoured in compounds **I**–**III** when compared with compounds **A**, **B** and **C**.

The mesophases observed for compounds **I**–**III** were identified based on optical textures observed under the optical microscope. Figure 3 shows the typical optical textures of the mesophases exhibited by these compounds. Compounds **I**–**III** exhibit textures characteristic for enantiotropic cholesteric (N*) and ferroelectric SmC* phases. On slowly cooling from the isotropic liquid, an oily streak and a fan texture characteristic of the cholesteric phase (N*) were observed (Figures 3(a) and 3(c)). The SmC* phase was identified by its characteristic iridescent petal (*47, 48*) and pseudo-homeotropic (*47*) textures (Figures 3(e) and 3(f)). The SmA phase present in compound **I** exhibited a fan-shaped texture coexisting with spherulitic regions (Figure 3(d)). An SmA phase, when consisting of chiral molecules, can adopt a helical ordering, thus forming a frustrated structure (TGBA) (*15, 49*). However, the texture observed for compound **I** is orthogonal SmA, where the molecules are arranged in layers so that their long axes are on average perpendicular to the diffuse layer planes. On the other hand, a platelet texture (Figure 3(b)) was

Downloaded At: 15:02 25 January 2011

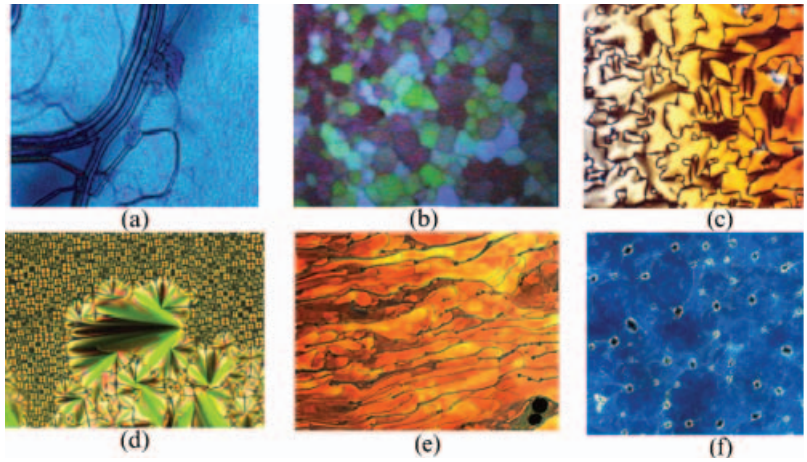

Figure 3. Photographs showing optical textures of compounds **I**–**III** taken during cooling: (a) oily-streak texture of the N* phase in compound **I** at 148°C; (b) platelet texture of the BP in compound **II** at 171°C; (c) fan texture of the N* in compound **II** at 156°C; (d) fan-shaped texture coexisting with spherulitic region of the SmA phase in compound **I** at 132°C; (e) iridescent petal texture of the SmC* phase in compound **II** at 146°C; (f) pseudo-homeotropic texture of the SmC* phase of compound **III** at 99°C.

Downloaded At: 15:02 25 January 2011

obtained for monotropic phase of the compounds **II** and **III**, which is consistent with a blue phase (BP).

X-ray diffraction studies

The three compounds (**I**–**III**) were studied by X-ray diffraction at high temperatures. In all cases, the diffractograms confirmed the nature of the mesophases identified by POM. The patterns recorded in the SmC* mesophase contain a sharp, strong maximum in the low-angle region, arising from the reflection of the X-ray beam on the smectic layers. The inter-layer spacing, *d*, was obtained by applying Bragg's law to this maximum, and the values obtained are presented in Table 2. In addition to this, the X-ray patterns contain a broad, diffuse halo in the high-angle region related with the short-range lateral correlations between neighbouring molecules in each layer. These correlations correspond to an average lateral distance of about 4.6 Å, and the diffuse character of this maximum is consistent with the liquid-like arrangement of the molecules within the smectic layer, as expected for a SmC mesophase. No other scattering maximum was detected in the patterns even after long exposure time, and therefore the liquid crystalline nature of the mesophases is unambiguously proven by the X-ray experiments.

The nematic nature of the high-temperature mesophase of the three compounds was confirmed by the presence in the X-ray patterns of diffuse scattering only. The absence of Bragg maxima is due to the lack of long-range positional order in the nematic phase, whereas the diffuse scattering arises from short-range correlations. The pattern of this mesophase contain two diffuse scattering maxima, one of them at low angles and the other at high angles, both of them located approximately at the same positions as the sharp reflection and the diffuse halo found in the SmC* mesophase. These diffuse maxima correspond to density fluctuations parallel and perpendicular to the long axis of the molecules, respectively, and arise from short-range intermolecular interactions along these two directions. This kind of pattern is classically found in all types of chiral and non-chiral nematic mesophases.

The SmA mesophase of compound **I** was also investigated and its nature confirmed by X-ray diffraction. The pattern is qualitatively similar to those recorded on the SmC* phase of the same

Table 2. Results of the X-ray experiments on the mesophases for compounds **I**–**III**. Parameter *d* represents the layer spacing in the SmC* and SmA mesophases or the wavelength of the density fluctuations in the N* mesophase (see discussion in the text). Parameter *L* is the molecule length estimated using ab initio calculation at HF/6-31 G(d) level. θ_L is the tilt angle calculated considering *L* as the molecule length (see text); θ_A is the tilt angle calculated considering the SmA layer spacing as the molecule length (see text).

Compound	Temperature/ °C	Phase	*d*/±0.5 Å	*L*/Å	θ_L/±2°	θ_A/±2°
I	95	SmC*	34	43.0	38	34
	136	SmA	41		–	–
II	118[a]	SmC*	32	43.3	42	38
	130	SmC*	33		40	36
III	100	SmC*	30	43.9	47	44
	130	N*	~32[b]		–	–

[a]Recorded in the cooling process. [b]Diffuse maximum.

compound, except for the shifting of the low-angle reflection to slightly lower angles, which means that the layer spacing becomes larger. This is the expected result, because in the SmA mesophase the molecules are orthogonal to the smectic planes, whereas they are tilted in the SmC* phase. Apart from the low-angle reflection, no other reflections are found in the X-ray pattern of the SmA mesophase, excepting a high-angle diffuse scattering halo characteristic of the liquid-like packing inside the layers. It is interesting to note that the SmC and the SmA mesophases are known to yield practically identical X-ray patterns, but they can easily be distinguished by their optical textures and by the different layer spacing.

A detailed variable-temperature study was performed for compound **I** (Table 3). For this study, an arrangement of the X-ray set-up was used that allows more accurate measurements in the small-angle region than those gathered in Table 2. The results of this study indicate that the layer spacing steadily increases upon heating within the thermal range of the SmC* phase and then there is a significant increase upon transition to the SmA phase. This behaviour is associated to a decreasing tilt angle in the SmC* phase as the temperature increases, followed by a reduction of the tilt angle to zero in the SmA phase.

The molecule length, L, of each of the three compounds was determined by means of *ab-initio* calculation at the HF/6-31G(d) level for an optimized conformation of the molecules (Table 2). By comparing these values with the measured layer spacing (d) the tilt angle could be deduced as $\theta_L = \cos^{-1} d/L$. The tilt angles θ_L calculated from this formula are gathered in Tables 2 and 3. By using this formula it is assumed that, in the mesophase, the molecules are in their most-extended conformation, i.e. with their hydrocarbon chains in the all-trans arrangement. However, this is probably not the case because in the SmA mesophase of compound **I** the measured layer spacing d is smaller by 2–2.4 Å than the molecule length L (Tables 2 and 3), in spite of the fact that the two values should be equivalent in an orthogonal smectic mesophase. This phenomenon has been found by us in other liquid crystal systems (*50*) and can be accounted for by the conformational disorder of the aliphatic chains. It can be safely deduced that in the SmC* mesophase of compound **I** the molecules do not adopt a fully-extended conformation and thus the actual molecule length is smaller than L and much close to the layer spacing d measured in the SmA mesophase. Therefore, the actual tilt should be more accurately calculated as $\theta_A = \cos^{-1} d_C/d_A$, where d_C and d_A are, respectively, the layer spacing measured in the SmC and SmA mesophases. The tilt angles θ_A calculated with this formula are also listed in Tables 2 and 3 and, as expected, they are smaller than those calculated with the above-mentioned formula based on the assumption of fully-extended molecules (θ_L).

Table 3. Results of the X-ray experiments on the mesophase of compound **I**. Parameter d represents the layer spacing in the SmC* (d_C) and SmA (d_A) mesophase. The molecule length L calculated using ab initio calculation at HF/6-31G(d) level is equal to 43.0 Å. θ_L is the tilt angle calculated considering L as the molecule length ($\theta_L = \cos^{-1}(d_C/L)$; θ_A is the tilt angle calculated considering the SmA layer spacing (40.6 Å) as the molecule length ($\theta_A = \cos^{-1}(d_C/d_A)$.

Temperature/°C	Phase	$d/\pm 0.3$Å	$\theta_L/\pm 1°$	$\theta_A/\pm 1°$
65	SmC*	32.4	41	37
70	SmC*	32.4	41	37
75	SmC*	32.9	40	36
80	SmC*	33.3	39	35
85	SmC*	33.6	39	34
90	SmC*	33.6	39	34
95	SmC*	33.9	38	33
100	SmC*	34.4	37	32
105	SmC*	34.9	36	31
110	SmC*	35.2	35	30
115	SmC*	35.6	34	29
120	SmC*	36.1	33	27
125	SmC*	37.0	31	23
130	SmC*	38.9	25	17
135	SmA	40.6	–	–
140	SmA	40.6	–	–
145	SmA	40.6	–	–
150	SmA	40.6	–	–

For compounds **II** and **III** it is not possible to calculate the tilt angle θ_A, using the formula based on the SmA layer spacing. However we can assume that, as in compound **I**, the molecule length in the mesophase is reduced by about 2–2.4 Å compared to the fully-extended length L, because the three compounds contain the same hydrocarbon chains (their mesogenic core is different but its contribution to the conformational freedom is not significant). Under this assumption, the formula $\theta_A = \cos^{-1} d_C/d_A$ can be applied to compounds **II** and **III**, where d_A is assumed to be 41 Å and 41.5 Å, respectively, and the obtained tilt angles are also gathered in Table 2. These values are more realistic than those previously calculated using the other formula for θ_L.

Finally, X-ray patterns were recorded of the solid phase that is obtained by cooling the SmC* mesophase of compound **II**. At first sight, the low value of the transition enthalpy (9.4 J g^{-1}) could suggest the possibility of another smectic phase, probably of high order (Table 1). However, the diffraction patterns indicate that this phase is crystalline, as revealed by the presence of a large number of sharp reflections over the whole angular range.

Downloaded At: 15:02 25 January 2011

Downloaded At: 15:02 25 January 2011

Ferroelectric properties

Ferroelectric properties were determined for compounds **I**–**III**. Figure 4 shows typical optical photomicrographs for the SmC* phase for compounds **I** and **III** between electrodes. For compound **I** (Figure 4(a)) the texture was achieved applying 40 V_{pp} with a 1 Hz triangular wave to the sample at 120°C in the SmC* phase. A fan-shaped texture, showing an equidistant line pattern due to the helical superstructure, was observed for this compound (see Figure 4(a), left side of the picture). The helix conformation in the absence of an electric field is one of the most characteristic textures in FLCs bearing a chiral centre. From the several adjacent lines observed it was possible to estimate the pitch of the helix, which in case of compound **I** was around 3.5 µm at 120°C. In case of compounds **II** and **III**, the estimated pitch was of 4.4 µm (130°C) and 2.8 µm (110°C), respectively. Figures 4(b) and 4(c) shows the situation when several electro-optical cycles were carried out for compounds **I** and **III**. On the left side of the electrode border, where the bias is applied, an electro-optical response is observed, whereas on the right side a region with no voltage treatment can be seen.

Ferroelectric properties of the samples were determined according to the methods previously described in the experimental section. When the samples were cooled slowly under a triangular-wave electric field, one polarization current peak for each half cycle could be obtained at a threshold of 60 V_{pp}, as soon as the SmC* phase was reached. The electro-optical current response trace obtained in the SmC* phase for compound **II** at 130°C is shown in Figure 5. This indicates that the lower temperature mesophase has a ferroelectric ground state structure. Table 4 summarizes the estimated properties for the investigated oxadiazoles.

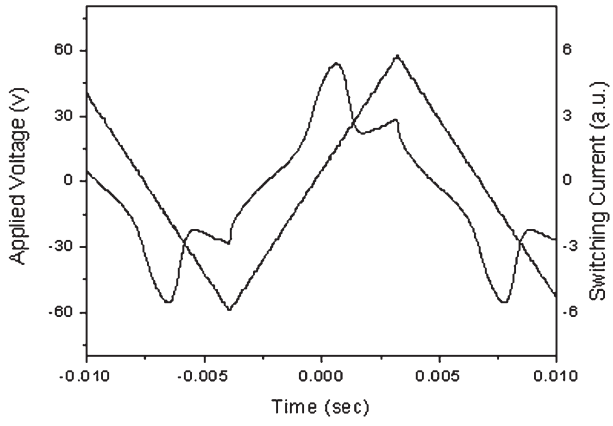

Figure 5. Switching current response trace obtained for compound **II** by applying a triangular-wave electric field (60 V_{pp}, frequency 70 Hz) in the SmC* phase at 130°C; cell thickness 6.8 µm.

Figure 6 shows the spontaneous polarization (Figure 6(a)) and the corresponding switching times (Figure 6(b)) evaluated from the electric displacement curves at different temperatures for compounds **I**–**III**. The maximum spontaneous polarization achieved was 144 nC cm^{-2} at around 135°C for compound **II**.

The temperature dependence of P_s is as expected, with an increase of the absolute value with a decrease in temperature, associated with the tilt angle variation inside the SmC phase. Nevertheless, a maximum is reached, with further gradual decrease in temperature, which finally results in a decreasing P_s that might at the beginning be due to a viscosity increase and afterwards sample crystallization. This effect is more pronounced in compound **II**, which is in good agreement with molecules possessing high ordered smectic phases. Other authors (*51*) describe that at the phase transition from fluid smectic phases to tilted hexatic phase, P_s values, tilt angle and helical pitch can suffer drastic deviation from linearity,

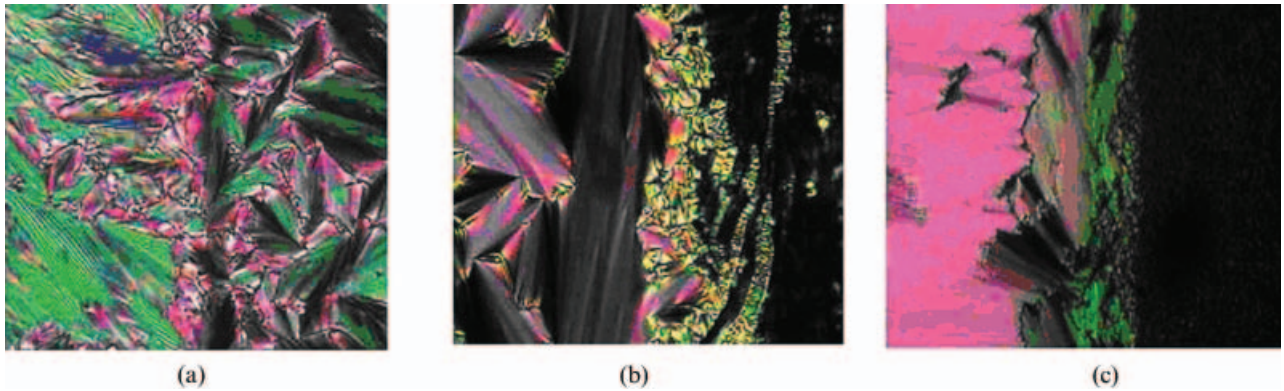

Figure 4. Observed texture for (a) compound **I** at 120°C, without bias, (b) compound **I** in SmC* phase (120°C), with 40 V_{pp} electric field applied and (c) compound **III** in SmC* phase (100°C) with 40 V_{pp} electric field applied. In all cases the electrode covers the left side of the picture.

Table 4. Ferroelectric properties in the SmC phase and calculated dipolar moment for compounds **I**–**III**.

Compound	P_s/nC cm^{-2}	τ_s/μs	V_{sat}/V μm^{-1}	Pitch/μm	θ/°	μ
I	60	50 (120°C)	13.24	3.5 (120°C)	41 (120°C)	3.78
II	144	200 (130°C)	8.83	4.4 (130°C)	43 (130°C)	5.72
III	65	200 (110°C)	8.82	2.8 (110°C)	38 (110°C)	4.44

P_s is the spontaneous polarization; τ_s is the switching time; V_{sat} is the saturation voltage; and θ is the tilt angle obtained from electrooptic measurements. μ is the calculated dipolar moment.

decreasing on cooling. This fact is concordant with the low value of the transition enthalpy of the SmC*–Cr transition of the compound **II** (see Table 1). We believe that the crystalline phase could be also a high ordered crystalline smectic tilted phase, with a strong restricted mobility, just appearing at the transition to the solid state. However, the temperature range of this mesophase was too small to investigate using X-ray diffraction.

The switching time is considerable faster than that which can be obtained with nematic materials. Typical switching times with pulse amplitudes of around 10 V μm^{-1} are of the order of 100 μs, which is about two orders of magnitude faster than nematic switching. This characteristic makes FLCs suitable for high-definition, highly multiplexed displays. For the compounds studied, the response time varies from 50 to 720 μs, which is in the expected range for these materials.

For all compounds the speed of switching has a nonlinear dependence on temperature. The increase in the time response is in good agreement with the decrease in temperature that must be associated with an increase in the viscosity of the mesophase. In compound **II** the switching process is rather fast (in the range of tens of milliseconds), which must be associated with the relatively large spontaneous polarization of 144 nC cm^{-2}.

From a structural point of view, the effect of the aromatic part of the mesogens in the mesomorphic properties is well evidenced due to the stabilization of the mesophase at higher temperatures in case of compounds **II** and **III** with respect to compound **I**. The latter does not possess a phenyloxy moiety and therefore a higher aliphatic character that increases flexibility can be recognized. Thus, a broader SmC temperature range is developed, that amounts almost 83°C and begins almost at room temperature. In this case the contribution to the spontaneous polarization is more related to the stabilization of the SmC phase than the chiral power of the compound.

The electronic structure of the oxadiazole fragment, which is influenced by the positions of its heteroatoms, plays a very important role in determining intra- and intermolecular interactions, which in turn may affect the molecular packing (*52*) and the ferroelectric properties. If we take into account that the chirality power corresponds to the (*S*)-4′-(1″-methylheptyloxy)-4-biphenylcarboxylate moiety, the 1,3,4-oxadiazole-2,5-yl fragment in compound **II** drastically enhances the total perpendicular dipolar moment. We believe that in this case, there is a strong coupling between both perpendicular dipoles in the molecule. On the other hand, the 1,2,4-oxadiazole-3,5-yl fragment in compound **III** diminishes the chiral

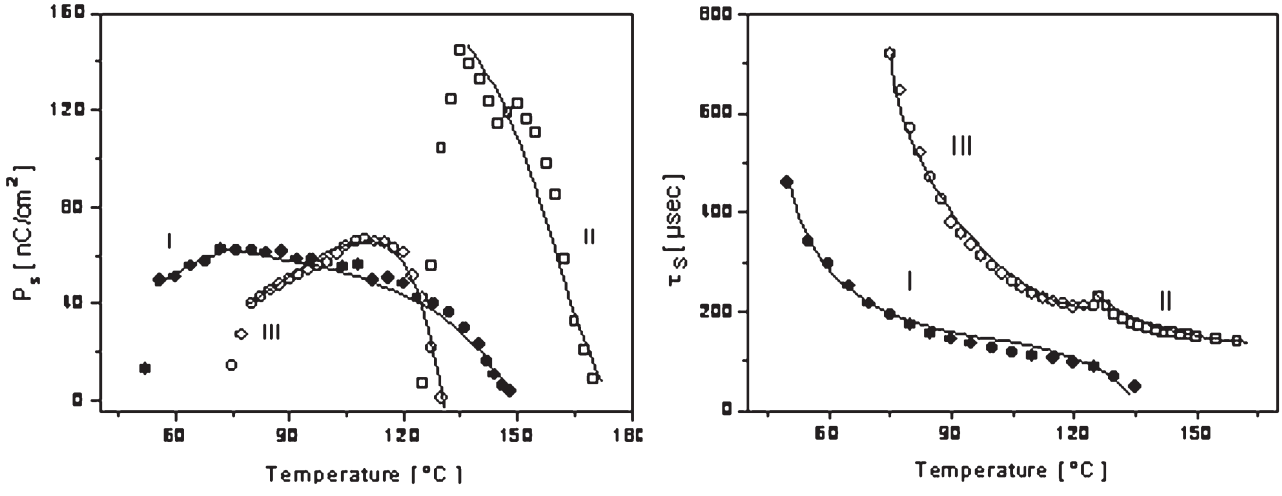

Figure 6. (a) Temperature-dependent spontaneous polarization and b) switching time for compound **I** (full circles), **II** (open squares) and **III** (open circles).

Downloaded At: 15:02 25 January 2011

power of the biphenylic moiety, perhaps due to the parallel longitudinal dipole of the heterocycle in the molecule. Theoretical calculations for the dipolar moment, by means of *ab-initio* calculation at the HF/6-31 G(d) level, for an optimized conformation of the molecules were carried out in all compounds and summarized in Table 4. Compound **II** shows the higher total dipole moment (5.72). The μx component of the dipolar moment in compound **III**, compared with compound **II**, is big and negative, which agrees well with our assumption relative to the longitudinal dipolar moment.

The tilt angle calculated from X-ray experiments using the theoretical value for the molecular length and the experimental one from the smectic A phase (Tables 2 and 3), was compared with the values obtained from electro-optical measurements, as summarized in Figure 7. The electro-optical data correlate well with the values that correspond to the longer tilt angles calculated from the observed interlayer distance. Thus, the reduced value for the interlayer distance in the SmA phase must be understood as a layer contraction due to some interdigitation of the layers at the interface or just the random movements of the terminal aliphatic chains. The differences in temperature are explained due to the different confinement for the sample, in one case inside a capillary and in the other case in a 6.8 µm thin sandwich cell.

Finally, electrical field dependence pyroelectric measurements were carried out in compound **I**, to corroborate our results. Temperature variations of the samples were caused by a modulated light from a semiconductor laser (λ=690 nm, P=27 mW, dc to 5 MHz), working at 70 Hz, provided from a function generator (HP 33120A, 0.1 MHz to 15 MHz). The sample was connected to a lock-in amplifier (EG&G Model 5460) operating in the voltage-sensitive mode (*53*). These results give a spontaneous polarization of around 54 nC cm^{-2}, slightly less, but comparable to that obtained from the repolarization current measurements.

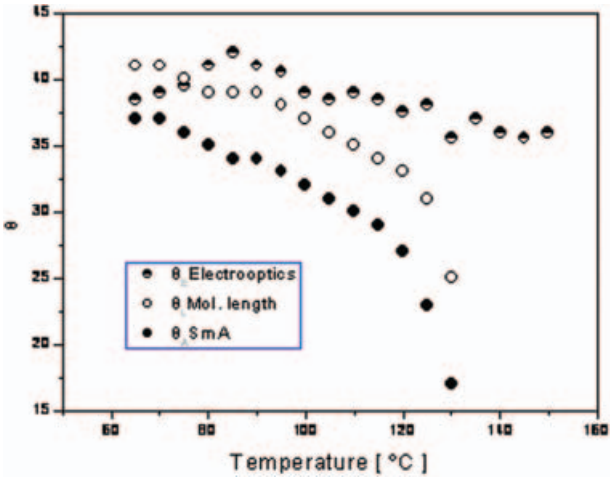

Figure 7. Tilt angles: θ_E is the tilt angle calculated from electro-optical measurements; θ_L is the tilt angle calculated considering L as the molecule length (see text); θ_A is the tilt angle calculated considering the SmA layer spacing as the molecule length (see text).

Conclusions

A study of the effect on physico-chemical properties of introducing oxadiazole fragments into the molecular core of three liquid crystals has been performed. The obtained results may provide a better understanding of the nature of liquid crystals and their use for various applications.

Examples of a new class of heterocyclic liquid crystals derived from oxadiazole were prepared, all of them showing enantiotropic liquid crystalline properties. Higher clearing point and wider ranges of phase temperatures were observed, where this enhanced effect can be attributed to stronger dipolar interactions coming from the heterocyclic fragments.

The structure of the heterocyclic fragment strongly affects not just the mesomorphic properties but also the ferroelectric characteristics of the material.

The 1,3,4-oxadiazolyl fragment seems to be the most promising family of compounds to develop high enough ferroelectric properties. Structural variations of compound **II** must be the next step in this investigation, directed in reducing the working temperature of the SmC phase in such compounds.

A high enough spontaneous polarization, together with a fast switching time, allows us to predict a promising field of investigation for the 1,3,4-oxadiazolyl FLC compounds.

Acknowledgements

We are grateful for financial support from FONDECYT 1030696 and 7060117 and ''Dirección de Investigación, Universidad de Concepción''.

References

(1) Clark N.A.; Lagerwall S.T. *Appl. Phys. Lett.* **1980**, *36*, 899–901.
(2) Goodby J.W. *J. Mater. Chem.* **1991**, *1*, 307–318.
(3) Goodby J.W.; Slaney A.J.; Booth C.J.; Nishiyama I.; Vuijk J.D.; Styring P.; Toyne K.J. *Mol. Cryst. Liq. Cryst.* **1994**, *243*, 231–298.
(4) Lunkwitz R.; Tschierske C.; Langhoff A.; Giebelmann F. *Liq. Cryst.* **1999**, *26*, 131–134.

Downloaded At: 15:02 25 January 2011

(5) Meyer R.B.; Liébert L.; Strzelecki L.; Keller P. *J. Phys. Lett.* **1975**, *36*, L69.
(6) Matsumoto T.; Fukuda A.; Johno M.; Motoyama Y.; Yui T.; Seomunc S.S.; Yamashitad M. *J. Mater. Chem.* **1999**, *9*, 2051–2080.
(7) Hegmann T.M.; Meadows R.; Wand M.D.; Lemieux R.P. *J. Mater. Chem.* **2004**, *14*, 185–190.
(8) McCubbin J.A.; Tong X.R.; Wang Y.Z.; Snieckus V.; Lemieux R.P. *J. Am. Chem. Soc.* **2004**, *126*, 1161–1167.
(9) Yablonskii S.V.; Soto-Bustamante E.A.; Vergara-Toloza R.O.; Haase W. *Adv. Mater.* **2004**, *16*, 1936–1940.
(10) Parra M.; Vergara J.; Zúñiga C.; Soto E.; Sierra T.; Serrano J.L. *Liq. Cryst.* **2005**, *32*, 457–462.
(11) Parra M.; Vergara J.; Hidalgo P.; Barberá J.; Sierra T. *Liq. Cryst.* **2006**, *33*, 739–745.
(12) Tschierske C.; Joachami D.; Zaschke H.; Kresse H.; Linstrom B.; Pelzi G.; Demus D. *Mol. Cryst. Liq. Cryst.* **1990**, *191*, 231–235.
(13) Yan X.; Baolong L.; Huibiao L.; Zijian G.; Zihou T.; Zheng X. *Liq. Cryst.* **2002**, *29*, 199–202.
(14) Iglesias R.; Serrano J.L.; Sierra T. *Liq. Cryst.* **1997**, *22*, 37–46.
(15) Gallardo H.; Ely F.; Bortoluzzi A.J.; Conte G. *Liq. Cryst.* **2005**, *32*, 667–671.
(16) Conte G.; Ely F.; Gallardo H. *Liq. Cryst.* **2005**, *32*, 1213–1222.
(17) Parra M.; Alderete J.; Zúñiga C.; Hidalgo P.; Vergara J.; Fuentes G. *Liq. Cryst.* **2002**, *29*, 1375–1382.
(18) Girdziunaite D.; Tschierske C.; Novotna E.; Kresse H. *Liq. Cryst.* **1991**, *10*, 397–407.
(19) Dimitrowa K.; Hauschild J.; Zaschke H.; Schubert H. *J. Prakt. Chem.* **1980**, *331*, 631–640.
(20) Sung H-H.; Lin H-Ch. *Liq. Cryst.* **2004**, *31*, 831–841.
(21) Dingemans T.J.; Samulski E.T. *Liq. Cryst.* **2000**, *27*, 131–136.
(22) Karamysheva L.A.; Torgova S.I.; Agafonova I.F.; Petrov V.F. *Liq. Cryst.* **2000**, *27*, 393–405.
(23) Semmler K.J.K.; Dingemans T.J.; Samulski E.T. *Liq. Cryst.* **1998**, *24*, 799–803.
(24) Hetzheim A.; Wasner C.; Werner J.; Kresse H.; Tschierske C. *Liq. Cryst.* **1999**, *26*, 885–891.
(25) Mochizuki H.; Hasui T.; Tsutsumi O.; Kanazawa A.; Shiono T.; Ikeda T.; Adachi C.; Taniguchi Y.; Shirota Y. *Mol. Cryst. Liq. Cryst.* **2001**, *365*, 129–138.
(26) Tokohisa H.; Era M.; Tsutsui T. *Adv. Mater.* **1998**, *10*, 404–407.
(27) Tokohisa H.; Era M.; Tsutsui T. *Chem. Lett.* **1997**, 303–304.
(28) Tokohisa H.; Era M.; Tsutsui T. *Appl. Phys. Lett.* **1998**, *72*, 2639–2641.
(29) Mochizuki H.; Hasui T.; Kawamoto M.; Shiono T.; Ikeda T.; Adachi C.; Taniguchi Y.; Shirota Y. *Chem. Commun.* **2000**, 1923–1924.
(30) Haristoy D.; Tsiourvas D. *Chem. Mater.* **2003**, *15*, 2079–2083.
(31) Lehmann M.; Köhn C.; Kresse H.; Vakhovskaya A. *Chem. Commun.* **2008**, 1768–1770.
(32) Tokuhisa H.; Era M.; Tsutsui T.; Saito S. *Appl. Phys. Lett.* **1995**, *66*, 3433–3435.
(33) Adachi C.; Tsutsui T.; Saito S. *Appl. Phys. Lett.* **1989**, *55*, 1489–1491.
(34) Hamada Y.; Adachi C.; Tsutsui T.; Saito S. *Jap. J. Appl. Phys.* **1992**, *31*, 1812–1816.
(35) Wagner H.J.; Loutfy R.O.; Hsiao C.K. *J. Mater. Sci.* **1982**, *17*, 2781–2785.
(36) Closs F.; Siemensmeyer K.; Frey K.; Funhoff D. *Liq. Cryst.* **1993**, *14*, 629–634.
(37) Parra M.; Fuentes G.; Vera V.; Villouta S.; Hernández S. *Bol. Soc. Chil. Quim.* **1995**, *40*, 455–460.
(38) Parra M.; Belmar J.; Zunza H.; Zúñiga C.; Fuentes G.; Martínez R. *J. Prakt. Chem.* **1995**, *337*, 239–241.
(39) Aguilera C.; Parra M.; Fuentes G. *Z. Naturforsch.* **1998**, *53b*, 367–370.
(40) Parra M.; Hidalgo P.; Carrasco E.; Barberá J.; Silvino L. *Liq. Cryst.* **2006**, *33*, 875–882.
(41) Torgova S.; Karamysheva L.; Strigazzi A. *Braz. J. Phys.* **2002**, *32*, 593–601.
(42) Parra M.L.; Hidalgo P.I.; Elgueta E.Y. *Liq. Cryst.* **2008**, *35*, 823–832.
(43) Merz W.J. *J. Appl. Phys.* **1956**, *27*, 938–940.
(44) Miyasato K.; Abe S.; Takezoe H.; Fukuda A.; Kuze E. *Jap. J. Appl. Phys.* **1983**, *L661*, 22–27.
(45) Mitsunobu O. *Synthesis* **1981**, *1*, 1–28.
(46) Torgova S.; Geinvandova T.; Francescangeli O.; Strigazzi A. *Pranama J. Phys.* **2003**, *61*, 385–393.
(47) Gray G.W.; Goodby J.W. *Smectic Liquid Crystals. Textures and Structures*; Leonard-Hill, Heyden and Son: Philadelphia, 1984.
(48) Cowling S.J.; Hall A.W.; Goodby J.W. *Liq. Cryst.* **2005**, *32*, 1483–1498.
(49) Goodby J.W.; Waugh M.A.; Stein S.M.; Chin E.; Pindak R.; Patel J.S. *J. Am. Chem. Soc.* **1989**, *111*, 8119–8125.
(50) Parra M.; Hidalgo P.; Barberá J.; Alderete J. *Liq. Cryst.* **2005**, *32*, 573–577.
(51) Glogarova M.; Novotna V.; Rytchetsky I.; Kaspar M.; Hamplova V. *Ferroelectrics* **2002**, *277*, 209–218.
(52) Osman M.A.; Revesz L. *Mol. Cryst. Liq. Cryst.* **1982**, *82*, 41–46.
(53) Soto-Bustamante E.A.; Navarrete-Encina P.A.; Weyrauch T.; Werner R. *Ferroelectrics* **2000**, *243*, 125–135.

Downloaded At: 15:02 25 January 2011